1   **Revision 1 Correction date 042417**

2   **Analysis of erionites from volcaniclastic sedimentary rocks and possible implications for**

3   **toxicological research.**

4   Martin Harper

5   Exposure assessment Branch, Health Effects Laboratory Division, National Institute for Occupational

6   Safety and Health, 1095 Willowdale Rd., MS-3030, Morgantown, WV 26505, USA

7   Alan Dozier

8   Chemical Exposure & Monitoring Branch, Division of Applied Research & Technology, National

9   Institute for Occupational Safety & Health, 1090 Tusculum Ave., MS-R7, Cincinnati, OH 45226, USA

10   Julie Chouinard

11   Center for Advanced Materials Characterization in Oregon (CAMCOR), University of Oregon, 1443 E.

12   13th Ave., Eugene, OR 97403, USA

13   Robyn Ray

14   EMSL Analytical, Inc., 200 Route 130 North, Cinnaminson, NJ 08077, USA

15

16   **Abstract**

17   Erionite occurs in volcaniclastic rocks and soils; in some villages in Turkey the presence of erionite in

18   local rocks is associated with mesothelioma, a disease also associated with inhalation of airborne

19   asbestos. Since volcaniclastic rocks containing erionite are widely present in the western USA, there is a

20   concern over potential health issues following inhalation of dust particles in these areas and thus there is

21   a need to identify and quantify erionite particles found in air samples during hygienic

22   investigations. Previous attempts to analyze the few micrometer-sized erionite particles found on air

23   sample filters under transmission electron microscope (TEM) encountered difficulties due to electron

24   beam damage.   Recommendations are presented for accurate analysis by both energy-dispersive

25   spectroscopy (EDS) and selected area electron diffraction (SAED). Much of the work previously

26   published to establish the crystal chemistry of erionite has involved the relatively large crystals found in

27   vesicles in extrusive volcanic rocks. Analysis of these crystals gives a weight percent ratio of Si to Al in

28   a narrow range around 2.7 (molar ratio 2.6), consistent with a unit cell formula $Al_{10}Si_{26}$. In addition, the

29   cation contents of these crystals generally meet the charge balance error formula for zeolites. However,

30   erionites formed in volcaniclastic sedimentary rocks (tuffs) have very different Si:Al weight percent

31   ratios, around 4.0, which is above the upper range for the analyses of the crystals found in vesicles.

32   Analysis of many particles in samples from different locations reveal two other major differences

33   between the erionites from the sedimentary situations and those found in vesicles. 1) The extra-

34   framework alkali cation (Na, K, Ca) contents are lower than required for a stoichiometric balance with

35   framework Al substitution for Si so that the cation charge balance error formula limits for zeolites are

36   not met. 2) There is a large variability in measured cation contents from particle to particle from the

37   same source as well as substantial differences in average compositions from different sources. However,

38   sedimentary erionites cannot be termed a separate mineral species because the crystallographic data are

39   consistent with erionite and new zeolite names cannot be proposed on the basis of Si:Al ratios alone. In

40   addition to chemical differences between erionite from different sources, there are also morphological

41   differences. By analogy with asbestos minerals, differences in composition and morphology may have

42   implications for relative toxicity, and future research should include consideration of these aspects.

43

44   KEYWORDS: ANALYSIS, CHEMICAL (MINERAL): erionite; ELECTRON MICROSCOPY:

45   erionite; MEDICAL MINERALOGY: erionite; Zeolites

46

47

48

Introduction

49

50   Erionite is a naturally occurring mineral that belongs to a group of silicate minerals called zeolites. It

51   was originally described from the Durkee opal mine near Durkee, Baker County, Oregon and named by

52   Eakle (1898). The name was derived from a Greek word that means wool because at the type locality the

53   erionite occurs as white, wool-like fibers. However, this is an uncommon habit, which has also been

54   observed in the Reese River zeolite deposits, near Austin, NV (Gude and Sheppard, 1981), but not

55   elsewhere. For more than half a century, this zeolite was considered extremely rare, and no additional

56   occurrences were listed until Deffeyes (1959) described material from Nevada and Wyoming. Unlike the

57   type erionite, these subsequent occurrences were either crystals formed in the vesicles of (mainly)

58   basaltic lavas, or microscopic, acicular to fibrous crystals in diagenetically altered, silicic, vitric tuffs of

59   Cenozoic lacustrine deposits (Mumpton and Ormsby, 1976). In most cases the erionite is likely to be a

60   later, pore-filling, re-crystallization of dissolved volcanic glass. Numerous additional discoveries of

61   erionite have been reported throughout the world, for example in many localities within the western

62   USA (Van Gosen et al., 2013). The large crystals found in the vesicles of mafic volcanic rocks have

63   been the materials most commonly examined when researching the crystallography and composition of

64   erionite. The standard published formula for erionite is $Al_{10}Si_{26}$, which gives a Si:Al wt % ratio of 2.7

65   (molar % ratio of 2.6). The average wt % value for the 25 different erionites analyzed by Passaglia et al.

66   (1998), all of which came from vesicles in volcanic rocks, using electron probe micro-analysis (EPMA)

67   was 2.6 (range 2.1-3.7). However, there are differences in major element (Si, Al) chemistry between

68   erionites from the two geological settings (vesicles in lavas and "sedimentary" deposits), and this was

69   noted by Gude and Sheppard in 1981. An examination of Figure 1 in Sheppard (1996) shows little

70   overlap in the Si:Al ratio between erionites from these two sources. Figure 1 of Sheppard (1996) also

71   shows most sedimentary erionites having Si:Al ratios greater than 3.3, up to around 3.8.

3

72 Erionite occurring in the "sedimentary" formations crystallizes as needle-like fibers of nanometer- to

73 micrometer-size widths. Larger bundles of these crystals are also common, often with a splayed

74 appearance. Disturbance of the friable rocks containing these microscopic crystals can generate airborne

75 fibers with physical dimensions similar to asbestos fibers. These particles may further resemble particles

76 of asbestos by exhibiting similar toxicity. For example, it has long been known that residents of some

77 Turkish villages where erionite-containing rock was used to construct homes have a remarkably high

78 risk for development of malignant mesothelioma (Baris et al. 1978; Rohl et al. 1982; Simonato et al.

79 1989; Baris 1991; Carbone et al., 2011). However, it should be noted that an early field survey by

80 Mumpton (1979) urged caution in the attribution: "*In so far as a positive correlation between the*

81 *occurrence of erionite or other zeolites in the tuffs from these Turkish villages and the incidence of*

82 *pleural mesothelioma, the data are equivocal, and tend to suggest that no correlation exists*." The

83 possibility exists that differences in chemistry and morphology of erionite found in different areas may

84 have consequences for toxicity.

85 Procedures are needed to identify erionite fibers in bulk rock, soil and air samples in order to assess the

86 potential for exposure and these procedures likely will include chemical analyses. In addition, an

87 understanding of the morphology and major and minor element chemistry of these particles is necessary

88 for the determination of factors that influence toxicity. Therefore, it is important that investigators be

89 aware of the differences between sedimentary erionite and the more classic crystals most often described

90 in the literature. However, the determination of chemistry of these microscopic crystals requires great

91 care. Previous analyses reported in the literature (Dogan and Dogan, 2008) appeared to meet the Mg %

92 requirement for erionite and the zeolite cation balance error formula, using the typical limitation (E <

93 10%). After recomputing, the reported analyses were found to be in error. A more recent publication

94 (Dogan, 2012) indicated "Among the 60 analyses …. only 3 passed both E% and Mg-content tests

95 (5.0%). This shows difficulty of quantitative characterization of the erionite series minerals." A

4

96   publication from the US Geological Survey (USGS) used a wider criterion for the balance error (E <

97   20%) to account for the obviously increased variance in the analyzed cation contents (Lowers et al.,

98   2010).

99   Prior to this study we had submitted fractions of the Rome, OR tuff to different commercial laboratories

100   for comparative analyses of fiber-like particles by TEM-EDS and SEM-EDS. However, very little

101   consistency was observed between laboratories. Some laboratories did not report important elements

102   (e.g. Na, Mg, Fe), giving as the reason that these elements were not observed above their limit of

103   detection, and one laboratory consistently reported high Fe in all samples. It became clear that higher

104   energies associated with TEM caused severe disruption to erionite crystals, resulting in physical

105   distortion (Figure 1), rapid loss of diffraction pattern, and a loss of "volatile" elements such as Na.

106   Depletion of alkali ions from glass under EPMA by migration to an electron-rich space charge layer has

107   been studied and corrections described for this phenomenon (Nielsen and Sigurdsson, 1981). A similar

108   effect was proposed for the loss of Na in the analysis of the zeolite, clinoptilolite, even after precautions

109   against loss had been taken (Broxton et al., 1987). Electron beam damage under electron microscopy is

110   also a well-known phenomenon, for example causing broadening and weakening of diffraction spots in

111   chrysotile (Zussman and Brindley, 1957) and charging and breakage of illite fibers (Purvis, 1991). Thus

112   there is a conflict between the high current and beam dose preferred to produce bright images and the

113   lower beam doses necessary to produce good diffraction patterns (Steel and Small, 1985). Just recently

114   beam damage has also been observed for relatively robust structures, such as amphibole asbestos

115   (Martin, et al., 2016). There are three major mechanisms of beam damage, known as knock-on

116   interaction ("sputtering") through elastic scattering (the same mechanism that results in diffraction

117   patterns), radiolysis, which is due to ionization through inelastic scattering (the same mechanism that

118   gives rise to EDS analyses), and electrostatic charging, although in many cases the last two mechanisms

119   cannot be distinguished, especially in the case of a highly intense and focused electron probe (Jiang and

120   Spence, 2012). The damage mechanisms have been studied to some extent in zeolites. A study of the

121   zeolite MCM-22 indicated that radiolysis dominates at low energies (<70 keV), and the damage depends

122   on the dose rate above a threshold irrespective of time of exposure, whereas at higher energies sputtering

123   also occurs and there is no threshold dose rate, the damage being a consequence of total dose, i.e. dose

124   rate times time of exposure (Ugurlu, et al., 2011). Since most TEM analyses are conducted at energies

125   around 100 keV or higher, both mechanisms are probably occurring.

126   In this work we confirm by selected area x-ray diffraction (SAED) of individual crystals that the

127   minerals we are examining are zeolites, specifically erionite. We present analyses of large numbers of

128   crystals by energy dispersive spectroscopy (EDS) using transmission electron microscopy (TEM), with

129   comparison to analyses by electron microprobe with wavelength dispersive spectroscopy (WDS). TEM-

130   EDS systems are readily available in many laboratories for commercial use; although electron

131   microprobe analyses are considered to be quite accurate when the analysis is performed properly, these

132   instruments are not common in industrial hygiene laboratories, and air-sample filters from hygienic

133   investigations are most likely to be analyzed by TEM, with EDS (and SAED). Finally, we also present

134   field-emission scanning electron microscopy (FE-SEM) and high resolution TEM (HR-TEM)

135   micrographs to illustrate the range of morphology in crystals from different locations.

136

137   **Materials**

138   Five samples of volcaniclastic sedimentary rock were obtained from various locations, primarily from

139   the western U.S. The material designated Rome was collected by the primary author in the vicinity of

140   the "Pillars of Rome", near Rome, OR. Material was selected from a specific horizon that contained ~

141   75% fibrous crystals by visual area estimation using a field optical microscope to examine the samples.

142   This was subsequently examined in the laboratory using confocal focusing techniques to evaluate the

143   three-dimensional geometry of all constituent particles in the tuff. The non-erionite material was almost

144   entirely volcanic glass. From the geometry of the different particles and assumed densities for erionite

145   and glass, the sample was determined to consist ~ 35% fibrous crystals by weight. This material is now

146   available in 10 gram aliquots for research purposes from RTI International (Research Triangle Park, NC;

147   contact Todd Ennis, jte@RTI.org). The material designated CGNF was collected by the primary author

148   from the Arikaree Formation of Palaeogene (Miocene-Oligocene) age from Reva Gap in the Slim Buttes

149   Land Unit of the Sioux Ranger District of the Custer-Gallatin National Forest, SD. This material

150   contained ~ 35% fibrous crystals by visual area estimation and using the same technique to convert from

151   area to mass as was used on the Rome material, ~ 1% by weight. Sub-samples of this material can also

152   be provided through contact with the primary author.

153   The material designated Killdeer was collected from the slope of South Killdeer Mountain, Dunn Co.,

154   ND. (Saini-Eidukat and Triplett, 2014) It is located approximately 75 miles from the Slim Buttes Land

155   Unit and is also believed to be from the Arikaree Formation. Area and weight percentages of fibrous

156   crystals were not determined for these samples, which are not available for further distribution. A small

157   quantity of a material designated Karain, from Cappadocia, Turkey was provided by International

158   Asbestos Testing Laboratories (IATL, Mt. Laurel, NJ, USA). The material designated Reese R. was

159   collected by the primary author from the Reese River zeolite deposit, Lander Co., NV. (Gude and

160   Sheppard, 1981) The erionite is reported to fills joints in gray to brownish-gray lacustrine mudstone of

161   probably Pliocene age. However, there is currently no outcrop and the material used in this work was

162   collected from the float in the indicated area of occurrence. It has the appearance of paper scraps, which

163   are clearly fibrous when broken. It is 100% erionite, with the same wooly appearance under the optical

164   microscope as that from Durkee, OR; these are the only two locations known where this particular habit

165   occurs in quantity. Macroscopic crystals of erionite were extracted from vesicles in a sample of volcanic

166   rock labelled "Ajo well #1 or Phelps Dodge Corporation Well #1, Ajo, Pima Co., AZ" from the primary

167   authors collection for comparison purposes. These were submitted for EPMA, but insufficient sample

168   was available for TEM-EDS, XRD or SAED analysis.

169

170   **Methods and Results – SAED**

171   For the SAED analyses, each sample was initially lightly ground in a mortar and pestle. The resulting

172   fine mineral powder was placed in a centrifuge tube and suspended with reagent alcohol (VWR

173   Analytical). The suspension was pipetted onto carbon coated 200 mesh copper TEM grids. Analysis

174   was conducted using a JEOL 1200 EXII transmission electron microscope (TEM) operated at 100 keV

175   and equipped with an IXRF Iridium EDXA and AMT side mount digital camera The electron beam's

176   intensity has been shown to rapidly decay the crystal lattice of zeolites. Therefore, the TEM grids were

177   mounted in a Gatan liquid nitrogen cooled double tilt TEM specimen holder. This holder keeps the

178   sample at -170 °C and helps to minimize the beam's impact on the crystal lattice thus preserving the

179   diffraction pattern for imaging and crystal zone indexing. From the diffraction patterns obtained,

180   indexing measurements were performed using the AMT software application to determine the miller

181   indices and zone axes. All fibers examined, including all 20 fibers in the first analysis from the bulk

182   CGNF sample, gave patterns consistent with erionite, however occasional fibers in this sample could

183   also be found with patterns indicating the possibility of an intergrowth with another mineral, this finding

184   is discussed in more detail under morphology. Variations were noted in the patterns between erionites

185   from different sources as shown in Figure 2. Killdeer patterns were weak and didn't last long. Karain

186   patterns were not as difficult to obtain as ND patterns, but were not as clear as those from Rome, CGNF

187   or Reese R. Finally, a CGNF sample was treated with 1:1 (50%) HCl and fibers under TEM showed no

188   discernable SAED patterns and also very little Al remaining under EDS.

189

190

8

Methods – EPMA

191

192 Seven samples of "sedimentary" erionite (Rome; CNF; Killdeer 3-01, 3-02 and 3-03; Karain; and Reese

193 R.) together with the vesicular erionite from Ajo, and National Institute of Standards and Technology

194 (NIST) reference zeolites were submitted for microprobe analysis at the University of Oregon.

195 Compositional analyses were acquired on an electron microprobe (Cameca SX100) equipped with five

196 tunable wavelength dispersive spectrometers and a 40° takeoff angle. A focused beam with an energy of

197 15 keV and current of 10 nA was used. Elements were acquired (all Kα lines) using an LiF analyzing

198 crystal for Fe, an LPET crystal for K and Ca, a TAP crystal for Na and Al, and an LTAP crystal for Si

199 and Mg. The standards utilized were synthetic MgO for Mg, synthetic SiO_2 for Si, NBS K-412 mineral

200 glass for Al and Fe, chlorapatite (halogen corrected) for Ca, nepheline for Na, and orthoclase for K. The

201 on-peak counting times were 40 seconds for K, 90 seconds for Si, Mg, and Ca, and 120 seconds for Na,

202 Al, and Fe. The off-peak correction method for K was linear with a counting time of 40 seconds; Na, Al,

203 Fe, Si, Mg, and Ca were background corrected using mean atomic number (MAN) intensity data which

204 were calibrated and continuum absorption corrected. Count intensities were corrected for deadtime and

205 standards were also corrected for any drift in intensity over time. A time dependent intensity (TDI) drift

206 correction was used for Na and K to account for any loss over time (Nielsen and Sigurdsson, 1981); both

207 elements were first tested to ensure their concentrations did not steeply drop off during the assigned

208 analysis time interval in order to avoid having an exponential fit to the TDI data. ZAF or Phi-Rho-Z

209 matrix corrections (Armstrong-Love/Scott algorithm; Armstrong, 1988) and the LINEMU mass

210 absorption coefficients dataset (Henke, 1985) were utilized. Oxygen was calculated by cation

211 stoichiometry and included in the matrix correction. Particles were selected for analysis on the basis of

212 having the appearance of fibers (aspect ratio > 3:1) and being at least 5 µm long, although actual size

213 measurements were not made. A trigonal prism particle correction (for curved top and flat sides or fiber

214 shaped materials), assuming a width of 1 µm, was used. The choice of width did not affect elemental

215   ratios or range of variability. Elemental analyses were normalized to 100% assuming no hydration

216   water. Approximately 20 particles were analyzed in each sample.

217   As the EPMA microscope did not include SAED, particles resembling fibers (aspect ratio > ~3:1, length

218   > ~5 μm) in the sedimentary zeolites were specially selected for these analyses. These were most likely

219   to be erionite, as confirmed by the separate SAED analyses. Occasionally, glass, clay minerals or

220   gypsum may appear as fibers under the microscope, however, their composition would be very different

221   from erionite. The NIST zeolite A reference material 8851 was used to test the analytical system. NIST

222   8851 has a 50% particle diameter of 2.24 μm measured by laser light scattering, which is similar to the

223   size of the sedimentary erionite particles, and had a similar response to the erionite particles during

224   analysis of Na. NIST zeolite Y reference material 8850 was also examined.

225

226   **Methods – TEM-EDS**

227   The analyses reported here used a 200 keV JEOL 2100F scanning transmission electron microscope

228   (STEM) with an Oxford Inca EDS attachment located at the NIOSH Alice Hamilton Laboratory in

229   Cincinnati, OH. The TEM-EDS systems limit of detection is considered to be two or three times the

230   background level, which usually will translate to 2 to 4 wt % composition depending on the energy and

231   noise level. Thus it can be quite difficult to obtain precise and accurate analyses of elements at < 1

232   weight%. Most, but not all of the same samples analyzed by EPMA were also submitted for TEM-EDS.

233   The NIST zeolite reference material 8851 was used to test the EDS system and determine the

234   microscope conditions necessary to limit electron beam exposure such that sodium in the reference

235   material (7.225 ±0.094% assuming full hydration; by x-ray fluorescence spectroscopy and instrumental

236   neutron activation analysis) was not affected. This reference material was considered by the analyst to

237   have a similar beam sensitivity to Na as erionite. Operating the TEM in the scanning transmission mode

238   using the smallest 0.2 nm probe available with the 25 μm condenser aperture gave the most comparable

10

239 analysis of Na to the reference composition in 8851. The sample was tilted 10° towards the EDS detector

240 to increase counts in order to obtain a satisfactory signal to noise ratio with a 100 second live count.

241 NIST 8850 was also used as a reference. It has a similar particle diameter to NIST 8851, but a lower

242 content of Na. The EDS data were processed with OXFORD software; GATAN software did not

243 produce as close a match to the reference material composition. Elemental analyses were normalized to

244 100% assuming no hydration water. For comparison with NIST reference compositions, the NIST

245 analyses were also normalized to 100% without water of hydration.

246 Ten fibers from each of the Rome, CGNF, and Karain (Turkey) samples were analyzed using this

247 procedure ("Old TEM" data in Table 2). Subsequently, comparison with the EPMA data suggested that

248 the EDS K percentage tended to be low, even though Na was unaffected. Repeat analyses of the Rome

249 and CGNF samples were performed where beam exposure was further reduced by limiting the

250 magnification to under 150,000x and by analyzing fibers $\geq$ 150 nm in diameter. Thirty Rome fibers, and

251 30 CGNF fibers from a sample sieved through screens designed to pass particles < 15 μm diameter (five

252 removed for Si> 40 wt%, but this did not affect the median ratio of Si:Al), were analyzed using the new

253 conditions and agreement with the microprobe data improved greatly ("New TEM" in Table 2).

254

255   **Results of chemical analyses**

256 Under EPMA, the average of 20 particles of NIST 8851 gave Si: 20 wt% (expected 20%); Al: 19%

257 (expected 19%); Na 15% (expected 16%). The coefficients of variation (CV) were 11% for Si, 17% for

258 Al, and 20% for Na. The average of 20 particles from NIST 8850 were Si: 31% (expected 30%); Al:

259 12% (expected 12%) and Na: 6.9% (expected 9.7%); the CV's were 5.9% for Si, 3.6% for Al, and 13%

260 for Na. The average of 10 particles from NIST 8851 analyzed under the optimized TEM-EDS conditions

261 gave Si: 23 wt% (expected 20%); Al: 22% (expected 19%); Na 15% (expected 16%). The coefficients of

262 variation (CV) were 11% for Si and Al, and 5.9% for Na. The average of 5 particles from NIST 8850

11

263   were Si: 34% (expected 30%); Al: 12% (expected 12%) and Na: 9.2% (expected 9.7%); the CV's were

264   2.8% for Si, 3.6% for Al, and 6.5% for Na.

265   The EPMA results from the sedimentary erionite samples are shown in Table 1. A very few individual

266   analyses were removed when calculating mean, median and standard deviation. Not removing these

267   analyses hardly affects the values, but by excluding those few analyses we feel the values are a more

268   accurate representation of the mean and median of the whole population. The number of analysis points

269   used is given in the table; the number not included were Rome (0); CNF (1); Killdeer 03-01 (8), 03-02

270   (4), 03-03 (4); Karain (0), Austin (0). Most of the data removed from consideration had very low Al

271   contents (< 6 wt%), except for one sample from CGNF (Si > 40 wt%), two from Killdeer 03-01 (one

272   with Fe > 8 wt% and one with Ca > 12 wt%), and one from Killdeer 03-02 (Al > 15 wt%). Under the

273   TEM it is possible to observe some fibers are associated with smaller particles on their surface. The

274   observational capability of the TEM usually allows these particles to be avoided in the analysis, but it is

275   more difficult do so in the microprobe. Therefore it is possible that some of the outlier chemistries are

276   the result of including associated particles in the analysis, for example, quartz (high Si), illite clay (high

277   Fe), or calcite (high Ca).

278   The Mg content of all these samples is low. A ternary plot (Figure 3) indicates that the majority of

279   analyses plot outside of the compositional field considered applicable to offretite. Table 2 provides a

280   comparison between EPMA and TEM-EDS of some useful metrics: Si/Al ratio, O wt% and cation wt%.

281   Note that these analyses, reported in wt% on a dry weight basis (assuming no water of hydration) should

282   not be compared directly with published analyses that have assumed (or in some cases, measured) water

283   of hydration. Repeat analysis of the Rome and CGNF samples with the additional restrictions noted

284   (designated new TEM) gave almost identical results under TEM-EDS to EPMA.

285

286

12

Discussion of chemical analyses

287

288   The NIST 8851 samples results are very comparable to the reference values using either EPMA or

289   TEM-EDS and the CV's are never greater than 20% and typically 12% or less. The CV's for TEM-EDS

290   are generally tighter than those with EPMA. The Pima Co. erionite under EPMA gave a Si:Al ratio of

291   2.66, as expected for an erionite from a vesicular lava. Negligible Na was present but the mean content

292   of Ca was 4.2% and the mean content of K 3.4%, both comparable to mean Ca and K percentages in

293   many of the sedimentary erionites analyzed. However, the CV's of Ca and K determinations in the Pima

294   Co. sample (Ca 16%, K 15%) were comparable to those of Na in the NIST reference materials and

295   generally much smaller than for the equivalent analyses of cations in the sedimentary erionites, which

296   ranged for most between 30 and 100%.

297   The Reese R. sample and the Turkish sample had Si:Al ratios, which, while high, are still within the

298   range reported previously for sedimentary erionites. However, there is a consistently higher Si:Al ratio,

299   3.9-4.0, in the other samples (Killdeer 03-01 samples, not listed in Table 2, also had a median Si:Al ratio

300   of 4.0), which is indicative of a unit cell of Al_6Si_{30}, rather than the classic unit cell of $Al_{10}Si_{26}$. Hay

301   (1964) noted that pH exerts a strong control over the silica content of crystallizing zeolites, with an

302   inverse correlation between the two. The smaller substitution of Si by Al in the structure of the erionites

303   from these localities requires fewer extra-framework cations for balance. Even so, none of these

304   analyses meet the cation charge balance error formula limits. Hydrogen ions compete with base cations

305   (Hay, 1966, p.78) and this competition may be enhanced at the lower pH of high-silica zeolite

306   formation. The extra-framework cation content also varies between localities, with the Rome sample

307   having the highest content. Finally, an extreme (order of magnitude) variation in any cation can be found

308   between two fibers in the same sample. The consistent picture between TEM-EDS and EPMA of low

309   extra-framework cation content and high variability does not appear to be related to a problem with the

310   analytical techniques. A possible geological explanation for these observations is very local ion-

13

311   exchange equilibria interactions with groundwater and possibly also other minerals within the rock.

312   Broxton et al. (1987) detailed variations in alkali and alkaline earth cation composition of clinoptilolite

313   over the geographical area they examined, and attributed the variation to mobilization during diagenesis

314   (i.e. formation of zeolite from volcanic glass), but they did not observe variation on the micro-scale

315   noted here. However, they only reported analyses that met the cation balance equation, discounting

316   others.

317   We believe the new TEM-EDS results have sufficient precision using the stated microscope conditions

318   that TEM-EDS systems can be used in the future to test for erionite presence, especially in combination

319   with other analytical methods such as SAED patterns obtained under low-temperature conditions,

320   provided similar quality systems to those described here are employed to ensure the accuracy of

321   analyses. Prior published analyses of erionite in these kinds of samples by TEM-EDS should be treated

322   with extreme caution, especially as there is no possibility of confirming them against an orthogonal

323   technique, such as inductively-coupled plasma optical-emission spectroscopy, when the microscopic

324   crystals make up only a few percent of the rock. This data set suggest that differentiation between K-,

325   Na- and Ca-erionites is not possible for the sedimentary erionites studied because of the cation content

326   variation within single samples.

327   It is interesting to note the large proportion of low-Al particles in the Killdeer samples compared with

328   the others. This difference in chemistry is not the result of analyzing other zeolites by mistake as no

329   other zeolites were identified by XRD in the bulk samples (Saini-Eidukat and Triplett, 2014 and current

330   data). In addition, the SAED patterns of Killdeer samples are typically very blurred compared to the

331   patterns from other samples. It should also be noted that loss of diffraction pattern and loss of Al was

332   apparent in our acidified sample of CGNF, suggesting that these Killdeer samples may have been

333   subjected to acidic groundwater at some point in their geological history (although we do not propose

334   that acidification after crystallization is the reason for the generally high Si:Al ratios in these samples).

14

335   This finding may have some bearing on the extra-framework cation contents of the minerals studied. In

336   laboratory studies of the cation-exchange capacity of other zeolites, Hoss and Roy (1960) noted: "The

337   data …. bring out the surprising fact that in many cases the cations do not appear to balance the charge

338   generated by Al3+ replacement of Si4+…. [while] Hydronium substitution in such samples could not be

339   proved conclusively …. Hydronium substitution is believed to take place easily …. Cation deficiency in

340   natural zeolites can be explained in the same way." However, it is the case that experimental proof for

341   such a hypothesis is lacking, and none is offered here.

342   Another interesting component of the chemistry is iron. In the CGNF samples, Killdeer and Reese R.

343   samples Fe is very low, typically less than 0.25%. However, by EPMA, 35% of Rome particles had >

344   2% Fe. Although this finding was not reproduced in our TEM-EDS analyses, it was also noted by

345   Matasso et al. (2015) in their analysis of Rome material. It is possible that this additional Fe is external

346   to the crystal as has been noted previously (Ballirano et al., 2009), and it may have been included in the

347   wider beam of our EPMA analyses. As noted above, particles adhering to the fibers were observed under

348   TEM and every effort was made to exclude them from the analysis and this may be why the Fe content

349   appears lower under our TEM analysis. The existence and location of Fe in these particles may be

350   important as it has been hypothesized that Fe may be a factor in the toxicity of erionite (Croce et al.,

351   2015).

352

353   **Morphology under Field-Emission SEM and High-Resolution TEM**

354   For analysis by Field-Emission (FE) SEM, particles were suspended in distilled water and filtered

355   through a 0.2 μm Nucleopore filter. The filters were trimmed and placed on an aluminum stub with

356   double-stick carbon tape and sputter-coated with gold-palladium and imaged with a, using a Hitachi S-

357   4800 FE-SEM operated at 5kV. Samples were also imaged with High-Resolution (HR) TEM, using a

358   FEI Tecnai G2 Twin TEM at an accelerating voltage of 200kV. Figure 4 shows FE-SEM images of

359   individual nano-fibrils around 40-60 nm wide, which were found in all samples, and which appear very

360   similar. However, the majority of fibers are much wider than these. In some case, this can be seen to be

361   because the fibers are bundles of thin fibrils, but this is not always the case. Figure 5 shows HR-TEM

362   images of Rome erionite side-by-side with CGNF erionite with contrasting morphologies. The Rome

363   erionite particle is clearly a bundle of the nano-width fibrils and the CGNF particle is a twisted ribbon-

364   like blade ~ 150 nm wide with no clear bundling of finer fibrils. Although as noted, individual nano-

365   width fibrils can be found in all samples, most of the CGNF particles more closely resemble the ribbon-

366   like blades, while most of the Rome particles appear as bundles. The morphology of the CGNF fibers

367   may be consistent with our diffraction data. Matassa et al. (2015) identified and measured two different

368   d-spacings in their sample of erionite from Durkee, OR, one perpendicular to the long axis of the fiber

369   and one parallel to the fiber elongation corresponding to $d_{002} = 0.747$ nm, and noted that the fibers they

370   observed also presented as ribbons. Thus the different spacing may only an artefact of fiber position,

371   rather than an intergrowth with another mineral; unfortunately it was not possible to tilt our stage to

372   investigate this further.

373   Additional differences between samples from different locations were apparent with a change in scale.

374   Under lower magnification, for example, CGNF erionite particles (fibers) are generally observed to be

375   longer (median 7 vs 5 μm) and wider (0.4 vs 0.3 μm) than Rome fibers, but with similar aspect ratio

376   (approx. 20:1), although the Rome sample often shows many short (~ 1 μm) fibers. The Karain, Turkey

377   sample is generally comprised of thinner fibers (~ 0.15 μm) as also noted by Lowers et al. (2010) and

378   the Reese R. sample is comprised of large bundles of nano-fibrils with a very wavy appearance (figure

379   6). The critical health outcome from exposure to airborne erionite is mesothelioma. In asbestos-related

380   disease, lung cancer occurs in association with mesothelioma, but that is not the case with erionite. It is

381   not known whether difference in particle sizes and morphologies between asbestos and erionite, and

382   between erionites from different locations effects health outcomes following exposure, but it may be so,

383   and further research is required, which should include a fuller analysis of mineral properties, as, for

384   example, in Mattioli et al. (2016).

385

386   **Discussion**

387   After careful analyses by microprobe-WDS and TEM-EDS, we agree with Dogan (2012) that the

388   analysis of erionite by TEM-EDS is difficult, but it can be optimized for identification and analysis.

389   Firstly, the EDS should be calibrated on NIST 8851, and/or 8850. Magnification should be kept below

390   150,000 x and particles analyzed should be wider than 150 nm. The beam should be the narrowest

391   available and dwell time must be limited. A minimum of 30 erionite particles should be studied per

392   sample by either TEM-EDS or EPMA to account for compositional variations between particles. Even

393   with careful consideration of these analytical parameters, we believe it is not possible to classify the

394   erionites we have studied from volcaniclastic sedimentary rocks as Na-, K-, or Ca-erionites because of

395   the large range of compositions between individual crystals. Macroscopic crystals of erionite formed in

396   magmatic vesicles match the "ideal" formula for erionite, but erionite crystals from volcaniclastic

397   sedimentary environments do not, being firstly poorer in aluminum, so requiring fewer extra-framework

398   cations for balance, and secondly being further depleted in cations over the number necessary to meet

399   the charge balance error formula (it is possible that the balance may be obtained through hydrogen ions,

400   although this was not studied). We believe these chemical differences to be a real reflection of either

401   different formational micro-environments or differences in the later diagenetic processes operating on a

402   micro-scale, but we do not believe it is because of uncertainty in the analytical techniques, since the

403   variation in the cation content from crystal to crystal is much greater than the analytical precision we

404   have confirmed using reference materials. Since the chemistry is so variable, SAED is a valuable

405   technique for more defensible erionite identification when other zeolite minerals could be present and a

406   cryogenically-cooled stage makes it possible to obtain these. The x-ray diffraction patterns of the

17

407 minerals we have studied here are consistent with erionite and the International Mineralogical

408 Association does not recognize new zeolite species on the basis of Si:Al ratio alone (Coombs et al.,

409 1997). Thus the analyses we present here, while unusual, cannot be construed to indicate a new mineral.

410 In addition to variations in chemistry within and between samples, there are considerable variations in

411 morphology. This variation in chemistry and morphology between samples from different locations may

412 have a bearing on relative toxicity, and this should be investigated further.

413

414 **Implications**

415 Erionite occurs in volcaniclastic rocks and soils; in some villages in Turkey the presence of erionite in

416 local rocks is associated with mesothelioma, a disease also associated with inhalation of airborne

417 asbestos. Since volcaniclastic rocks containing erionite are widely present in the western USA, there is a

418 concern over potential health issues following inhalation of dust particles in these areas and thus there is

419 a need to identify and quantify erionite particles found in air samples during hygienic

420 investigations. Previous attempts to analyze the few micrometer-sized erionite particles found on air

421 sample filters under transmission electron microscope (TEM) encountered difficulties due to electron

422 beam damage.   Recommendations are presented for accurate analysis by both energy-dispersive

423 spectroscopy (EDS) and selected area electron diffraction (SAED) and these recommendations will be

424 incorporated into consensus standard methods under development. In addition, our analytical findings

425 have implications for current and future studies on the toxicity of erionite. Differences in the relative

426 toxicity of asbestos minerals have been related to variations in composition and morphology. It is

427 possible that the variation in volcaniclastic erionite composition and morphology between localities we

428 have found may have an analogous bearing on toxicity, and this should be investigated further. The

429 major differences between erionites from magmatic vesicles and those that have crystallized in

430 volcaniclastic sedimentary rocks needs to be fully recognized. Further, the particle-to-particle variation

431 in cation chemistry has implications for the interpretation of prior studies that have examined few, or

432 only single, particles.

433

434

435

436   **Acknowledgements**

441

442 **Disclaimer:** The findings and conclusion in this report are those of the author(s) and do not necessarily

443 represent the official position of the National Institute for Occupational Safety and Health.

444

445 **References**

446 Armstrong, J.T. (1988) Quantitative analysis of silicates and oxide minerals: Comparison of Monte-

447 Carlo, ZAF and Phi-Rho-Z procedures. Microbeam Analysis, 239-246.

448 Ballirano, P. Andreozzi, G.B., Dogan, M. and Dogan, A.U. (2009) Crystal structure and iron

449 topochemistry of erionite-K from Rome, Oregon, U.S.A. American Mineralogist, 94, 1262-1270.

450 Baris, Y.I. (1991) Fibrous zeolite (erionite)-related diseases in Turkey. American Journal of Industrial

451 Medicine, 19, 374-378.

452 Baris, Y.I., Sahin, A.A., Ozesmi, M., Kerse, I., Ozen, E., Kolacan, B., Alinörs, M. and Göktepeli, A.

453 (1978) An outbreak of pleural mesothelioma and chronic fibrosing pleurisy in the village of

454 Karain/Urgup in Anatolia. Thorax, 33, 181-192.

19

455   Broxton, D.E., Bish, D.L. and Warren, R.G. (1987) Distribution and chemistry of diagenetic minerals at

456   Yucca Mountain, Nye County, Nevada. Clays and Clay Minerals, 35, 89-110.

457   Carbone, M., Baris¸, Y. I., Bertino, P., Brass, B., Comertpay, S., Dogan, A.U., Gaudino, G., Jube, S.,

458   Kanodia, S., Partridge, C.R., Pass, H.I., Rivera, Z.S., Steele, I., Tuncer, M., Way, S., Yang, H. and

459   Miller, A. (2011) Erionite exposure in North Dakota and Turkish villages with mesothelioma.

460   Proceedings of the National Academy of Sciences, 108(33), 13618–13623.

461   Coombs, D.S., Alberti, A., Armbruster, T. Collela, C., Galli, E., Grice, J.D., Liebau, F., Mandarino, J.A.,

462   Minato, H., Nickel, E.H., Passaglia, E., Peacor, D.R., Quartieri, S., Rinaldo, R., Ross, M., Sheppard,

463   R.A., Tillmanns, E. and Vezzalini, G. (1997) Recommended nomenclature for zeolite minerals: report of

464   the subcommittee on zeolites of the international mineralogical association, commission on new

465   minerals and mineral names. Canadian Mineralogist, 35, 1571-1606.

466   Croce, A., Allegrina, M. Rinaudo, C., Gaudino, G., Yang, H. and Carbone, M. (2015) Numerous iron-

467   rich particles lie on the surface of erionite fibers from Rome (Oregon, USA) and Karlik (Cappadocia,

468   Turkey). Microscopy and Microanalysis, 21, 1341-1347.

469   Deffeyes, K.S. (1959) Erionite from Cenozoic tuffaceous sediments, central Nevada. American

470   Mineralogist, 44, 501-509.

471   Dogan, A.U. and Dogan M. (2008) Re-evaluation and re-classification of erionite series minerals.

472   Environmental Geochemistry and Health, 30, 355-366.

473   Dogan, M. (2012) Quantitative characterization of the mesothelioma-Inducing erionite series minerals

474   by transmission electron microscopy and energy dispersive spectroscopy. Scanning, 34, 37-42.

475   Eakle, A.S. (1898) Erionite, a new zeolite. American Journal of Science, 6, 66-68.

476   Gude, A.J. and Sheppard R.A. (1981) Woolly erionite from the Reese River zeolite deposit, Lander

477   County, Nevada, and its relationship to other erionites. Clays and Clay Minerals, 29, 378-384.

478   Hay, R.L. (1964) Phillipsite of saline lakes and soils. American Mineralogist, 49, 1366-1387.

479   Hay, R.L. (1966) Zeolites and zeolitic reactions in sedimentary rocks. Geological Society of America

480   Special Paper, 85, NY, 130 pp.

481   Henke, B.L. (1985) Scattering factors and mass absorption coefficients. Chapter 2.7 in X-ray Data

482   Booklet (D. Vaughan, ed.) Center for X-ray Optics, Lawrence Berkeley Laboratory, Berkeley, CA.

483   Hoss, H. and Roy, R. (1960) Zeolite Studies III: On natural phillipsite, gismondite, harmatome,

484   chabazite, and gmelinite. Beiträge zur Mineralogieund Petrographie, 7, 389-408.

485   Jiang, N. and Spence, J.C.H. (2012) On the dose-rate threshold of beam damage in TEM.

486   Ultramicroscopy 113, 78-82.

487   Lowers, H.A., Adams, D.T., Meeker, G.P. and Nutt, C.J. (2010) Chemical and Morphological

488   Comparison of Erionite from Oregon, North Dakota, and Turkey. US Geological Survey Open-File

489   Report 2010–1286, USGS, Reston, VA.

490   Martin, J., Beauparlant, M., Sauvé, S. and Espérance, G. (2016) On the threshold conditions for electron

491   beam damage of asbestos amosite fibers in the transmission electron microscope (TEM). Journal of

492   Occupational and Environmental Hygiene, 12, 924-935.

493   Matassa, R., Familiari, G., Relucenti, M., Battaglione, E., Downing, C., Pacella, A., Cametti, G. and

494   Ballirano, P. (2015) A deep look into erionite fibres: an electron microscopy investigation of their self-

495   assembly. Scientific Reports, 5, 16757.

496   Mattioli, M., Giordani, M., Dogan, M., Cangiotti, M., Avella, G., Giorgi, R., Dogan, A. U., and

497   Ottaviani, M.F. (2016) Morpho-chemical characterization and surface properties of carcinogenic zeolite

498   fibers. Journal of Hazardous Materials, 305, 140–148.

499   Mumpton, F.A. (1979) Reconnaissance study of the association of zeolites with mesothelioma cancer

500   occurrences in central Turkey. Society of Mining Engineers of AIME Preprint Number 79-332,

501   presented at SME-AIME Fall Meeting, Tucson, AZ, October 17-19, 23 pp.

502   Mumpton, F.A. and Ormsby, W.C. (1976) Morphology of zeolites in sedimentary rocks by scanning

503   electron microscopy. Clays and Clay Minerals, 24, 1-23.

504   Nielsen, C.H. and Sigurdsson, H. (1981) Quantitative methods for electron microprobe analysis of

505   sodium in in natural and synthetic glasses. American Mineralogist, 66, 547-552.

506   Passaglia, E., Artioli, G., Gualtieri, A. [1998] Crystal chemistry of the zeolites erionite and offretite.

507   American Mineralogist, 83, 577-589.

508   Purvis, K. [1991] Fibrous clay mineral collapse produced by beam damage of carbon-coated samples

509   during scanning electron microscopy. Clay Minerals, 26, 141-145.

510   Rohl, A.N., Langer, A.M., Moncure, G., Selikoff, I.J. and Fischbein. A. (1982) Endemic pleural disease

511   associated with exposure to mixed fibrous dust in Turkey. Science, 216, 518-520.

512   Saini-Eidukat, B. and Triplett, J.W. (2014) Erionite and offretite from the Killdeer Mountains, Dunn

513   County, North Dakota, U.S.A. American Mineralogist, 99, 8–15.

514   Sheppard R.A. Occurrences of Erionite in Sedimentary Rocks of the Western United States. US

515   Department of the Interior, US Geological Survey Open-File Report 96-018. Denver, CO, 1996, 24 pp.

516   Simonato, L., Baris, R., Saracci. R., Skidmore, J. and Winkelmann R. (1989) Relation of environmental

517   exposure to erionite fibres to risk of respiratory cancer. International Agency for Research on Cancer

518   (IARC) Scientific Publications, 90, 398-405.

519   Steel, E.B. and Small, J.A. (1985) Accuracy of Transmission Electron Microscopy for the analysis of

520   asbestos in ambient environments. Analytical Chemistry, 57, 209-213.

521   Ugurlu, O., Haus, J., Thomas, M.G. Maheshwari, S., Tsapitis, M. and Mkhoyan, K.A. (2011) Radiolysis

522   to knock-on damage transition in zeolites under electron beam irradiation. Physics Reviews B, 83,

523   113408(1-4).

22

524   Van Gosen, B. S., Blitz, T.A., Plumlee, G.S., Meeker, G.P. and Pierson, M.P. (2013) Geologic

525   occurrences of erionite in the United States: an emerging national public health concern for respiratory

526   disease. Environmental Geochemistry and Health 35(4), 419-430.

527   Zusmann, J. and Brindley, G.W. (1957) Electron diffraction studies of serpentine minerals. American

528   Mineralogist, 42, 133-153.

529

530

531 Table 1 EPMA analyses (elemental weight %, dry weight basis) of fibers from rock samples. ND (Killdeer) sample

532 numbers refer to horizons in Saini-Eidukat and Triplett (2014). (Med. = median, CV =coefficient of variation)

	Si				Al				Mg			Fe		
	Low	High	Med.	CV%	Low	High	Med.	CV%	Low	High	Med.	Low	High	Med.
Karain (n=19)	30	36	34	6.0	6.4	10	8.9	12	0.51	2.5	0.77	0.16	6.2	0.34
Rome (17)	25	36	32	10	6.9	11	7.9	13	0.12	3.9	1.0	0.48	7.1	1.4
ND 03-01 (10)	29	36	34	6.8	6.1	14	8.9	30	0.19	3.5	0.87	0.16	4.6	0.27
ND 03-02 (16)	33	37	35	2.9	6.8	10	8.3	13	0.17	1.7	0.59	0.10	1.3	0.14
ND 03-03 (11)	30	39	36	6.9	6.9	13	9.0	22	0.10	1.0	0.66	0.08	0.42	0.17
CGNF (19)	24	37	34	11	6.7	13	8.3	17	0.58	2.7	1.2	0.27	3.0	0.55
Reese R. (17)	26	36	33	7.7	6.6	13	9.5	14	0.18	2.0	0.27	0.11	4.9	0.44

533

534

535

	Na			K			Ca		
	Low	High	Median	Low	High	Median	Low	High	Median
Karain (n=19)	0.75	4.8	1.8	2.7	4.6	3.6	1.1	2.8	1.4
Rome, OR (17)	0.25	4.6	0.54	1.5	5.9	4.4	0.61	7.3	4.5
ND 03-01 (10)	0.1	1.7	0.3	2.3	5.0	3.2	1.1	4.5	2.0
ND 03-02 (16)	0.02	1.3	0.07	1.9	3.7	2.7	2.6	3.8	3.3
ND 03-03 (11)	0.1	0.6	0.34	0.03	4.0	2.5	0.01	3.4	2.4
CGNF (19)	0	5.1	0.87	1.0	4.4	3.1	1.3	11	1.8
Reese R. (17)	0.16	0.55	0.25	1.5	6.5	3.1	2.0	7.8	4.0

536   Table 2 Median values of Si:Al ratios and elemental weight % compositions (dry weight basis) from different

537   analytical techniques.

538

	Si:Al ratio		Oxygen wt%		Ca wt%		K wt%		Na wt%	
	Microprobe	TEM	Microprobe	TEM	Microprobe	TEM	Microprobe	TEM	Microprobe	TEM
Rome (microprobe17/ Old TEM10)	3.9	4.0	48	51	4.5	3.2	4.4	1.9	0.4	0
Rome New TEM (30)		4.0		45		3.4		4.3		0
CGNF (microprobe19/ Old TEM10)	3.9	4.0	49	52	1.8	1.3	3.1	1.7	0.9	0.4
CGNF New TEM (24)		3.9		47		1.5		3.8		0.9
Karain (microprobe19/ Old TEM11)	3.8	3.4	49	43	1.4	1.1	3.6	4.7	1.8	1.9

539

26

540   Figure 1. Distortion of an erionite crystal with increasing time under 100 keV TEM beam energy. Photographs

541   courtesy of IATL.
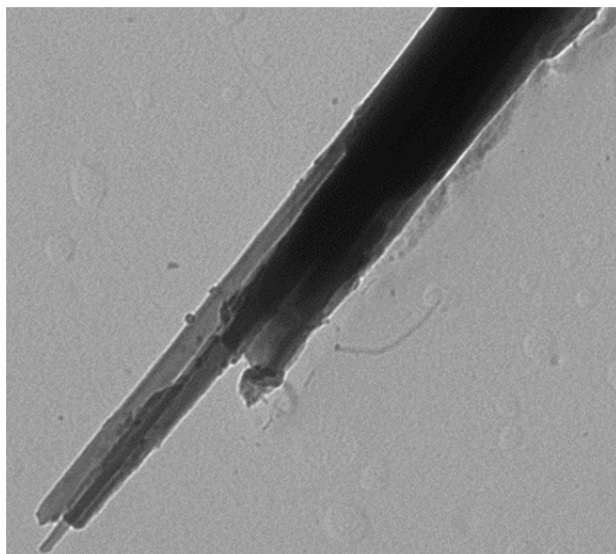
542

543   1(a) with beam first applied. Scale: particle is approximately 300 nm wide at thickest point.
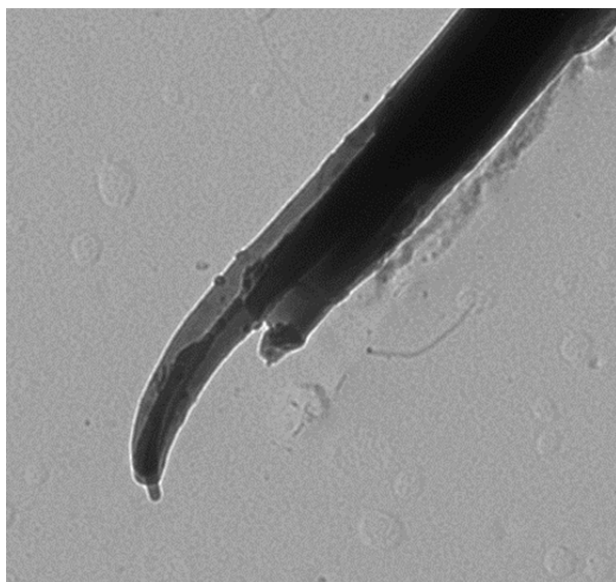
544

545   1(b) same particle after collection of diffraction data

546   Figure 2. SAED of erionite particles

547   a) Rome, OR

548

549

550

28

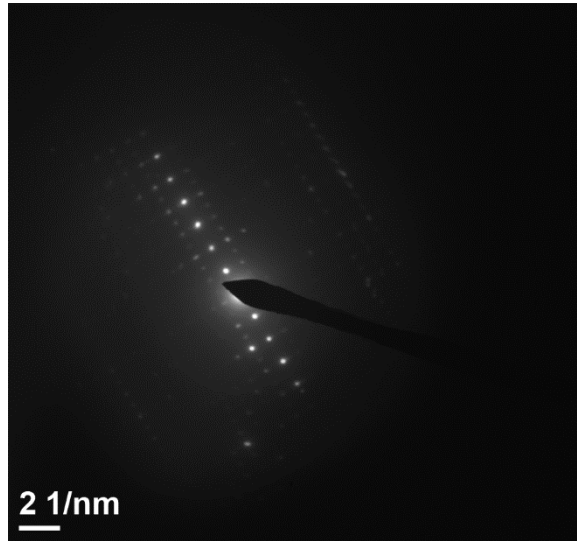551   b) CGNF, SD

2 1/nm

552

553

29
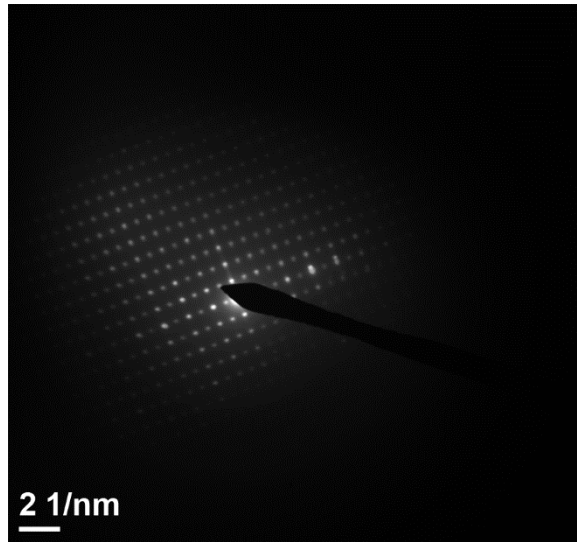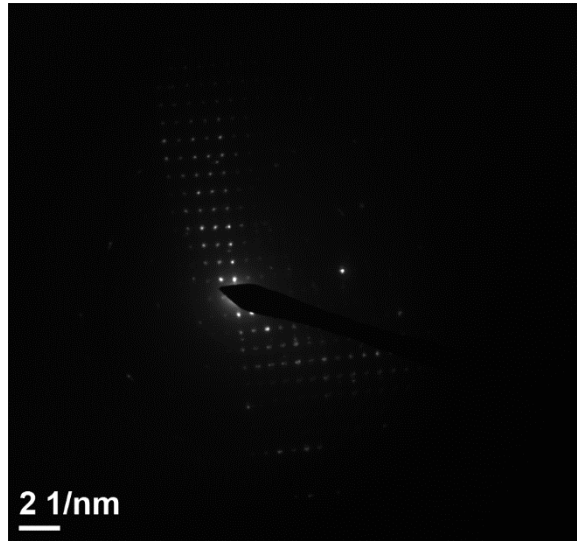
554   c) Killdeer 03-03, ND

555

2 1/nm
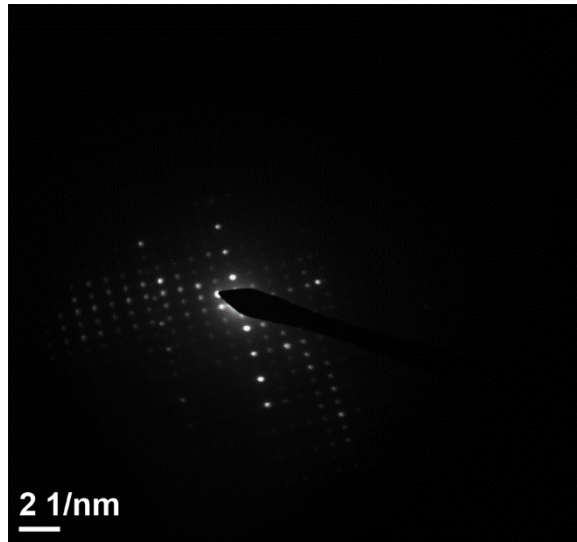
556

557

558   d) Karain, Turkey

559

560

561   e) Reese R., NV

562
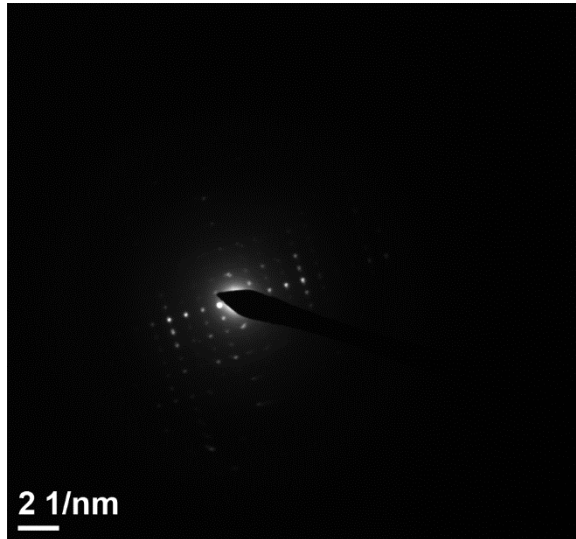
563   Figure 3 Ternary plot of all erionite analyses (red circle is approximate compositional field for offretite –
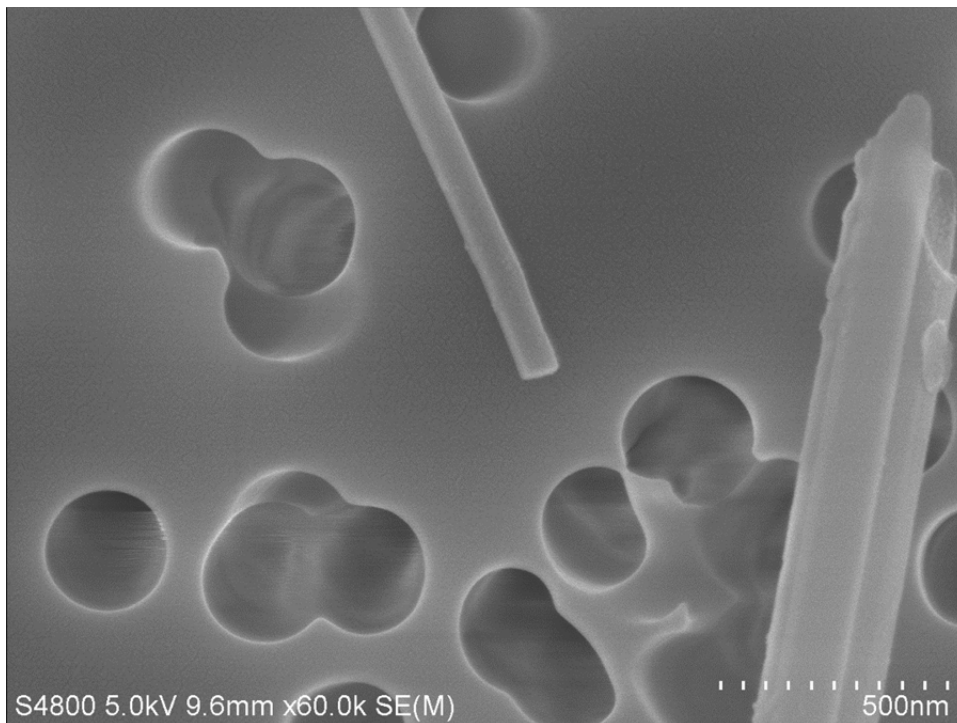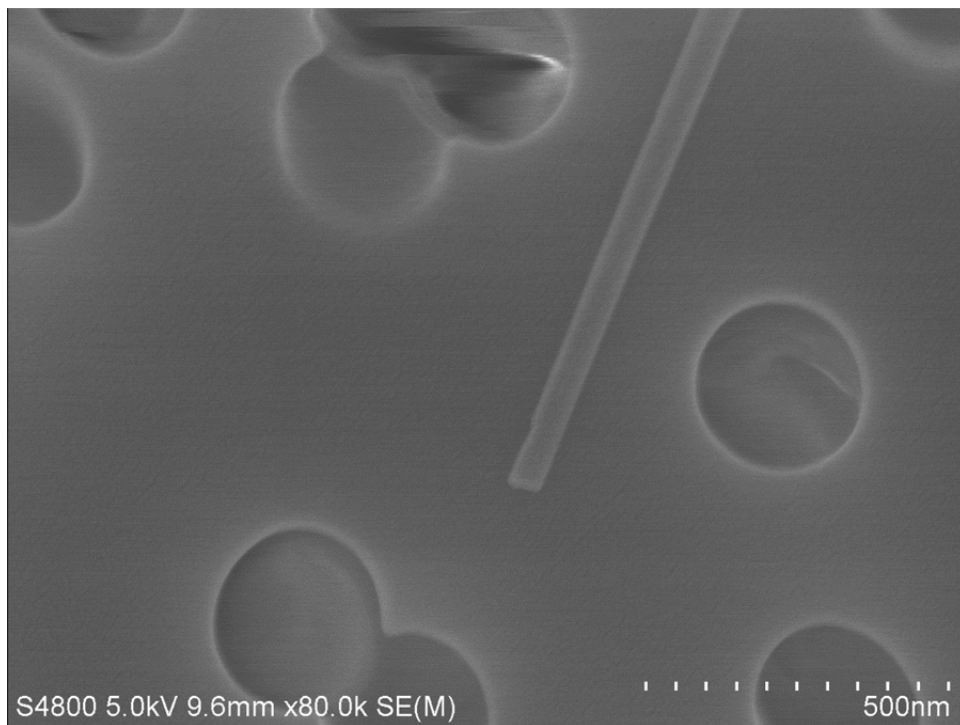
564   Passaglia et al. 1998)

565
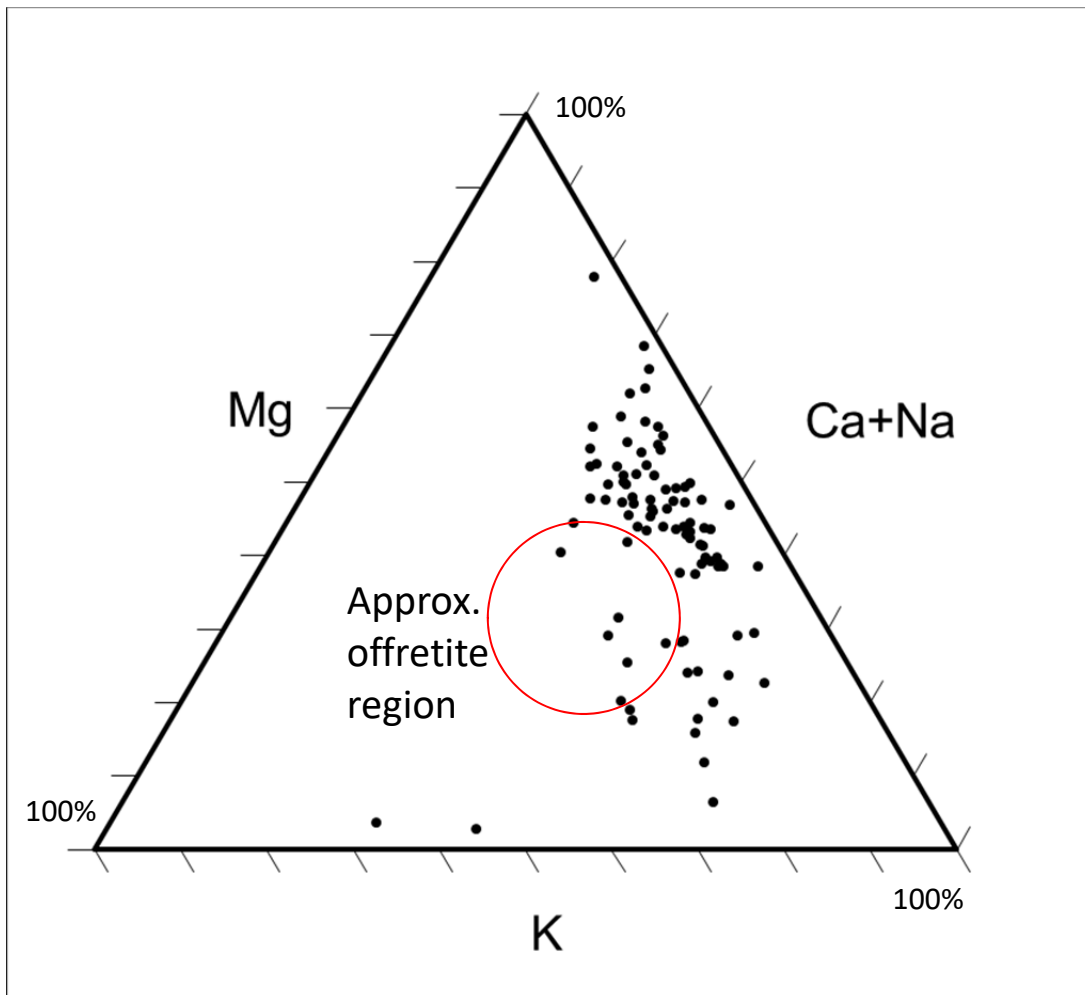
566

567   Figure 4 FE-SEM images of individual erionite fibrils from different samples: a) Rome, b) CGNF, c) Karain, d)
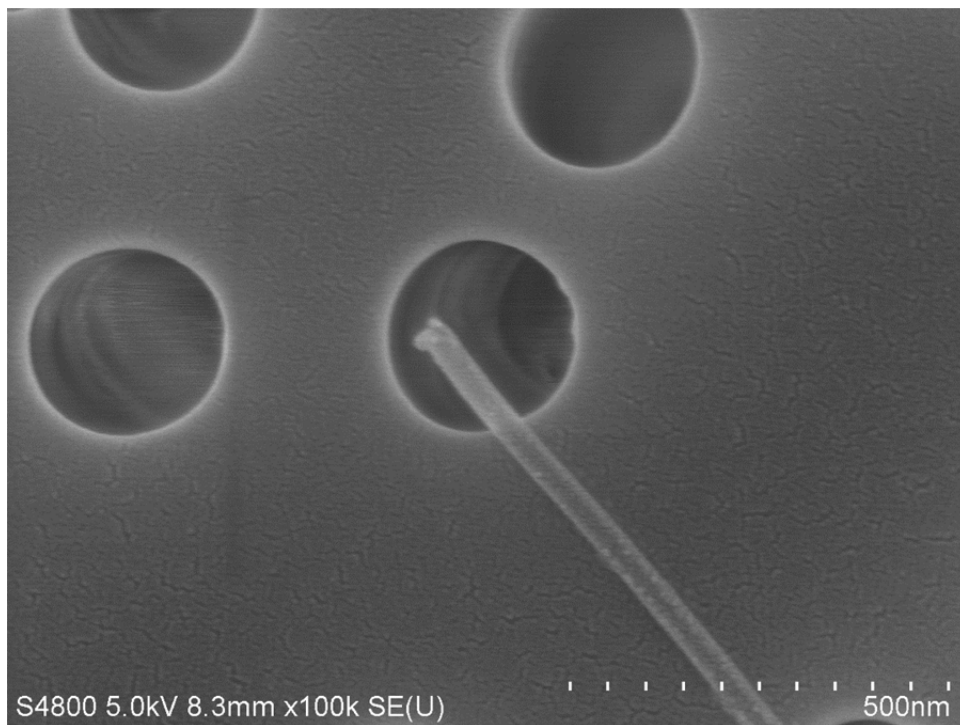
568   Killdeer

569   a)
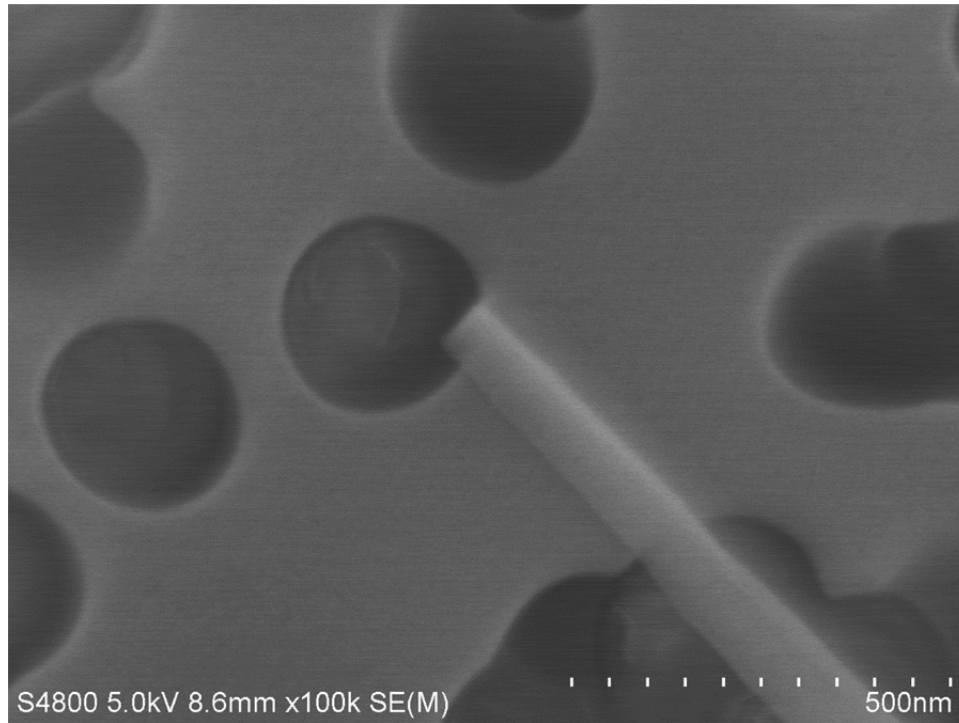

570

S4800 5.0kV 9.6mm x60.0k SE(M)   500nm

571

572   b)

S4800 5.0kV 9.6mm x80.0k SE(M)   500nm

573

574

35

575   c)

S4800 5.0kV 8.3mm x100k SE(U)   500nm

576

577

578   d)

579

S4800 5.0kV 8.6mm x100k SE(M)   500nm
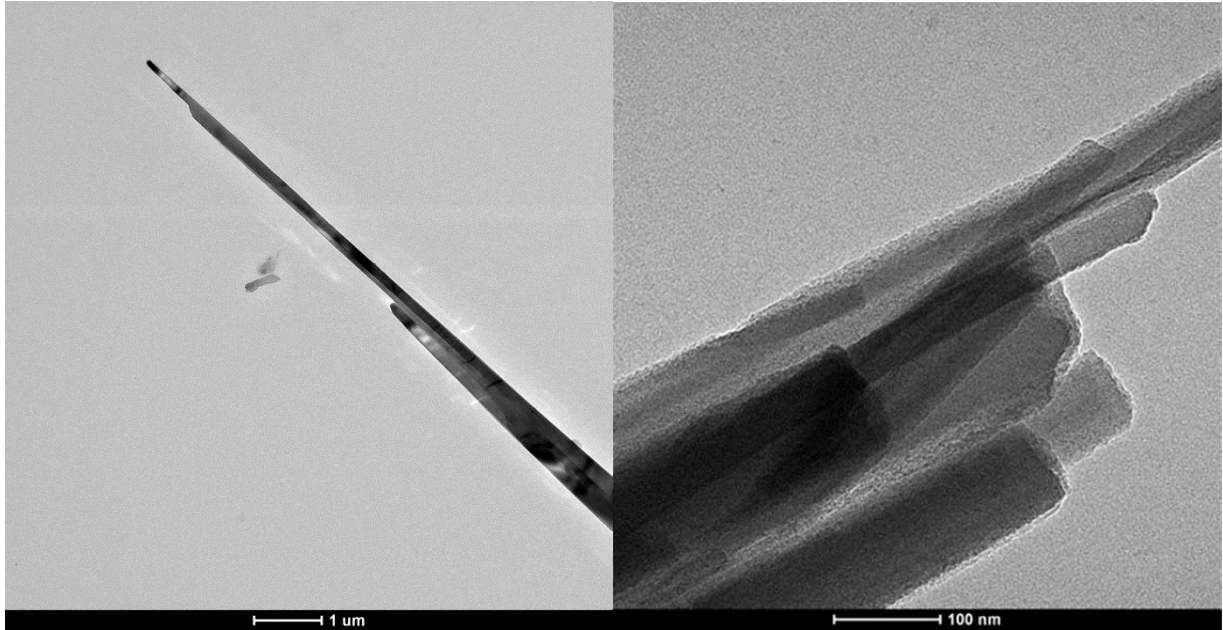
580

581   Figure 5 HR-TEM images of CGNF and Rome fibers side-by-side (note difference in scale)

582

583   (a) CGNF, (b) Rome

584

585   Figure 6. "Wooly" erionite from Reese River, NV (FE-SEM)

586

39